Comparison of CAMRAD II and RCAS Predictions of Tiltrotor Aeroelastic Stability

Hyeonsoo Yeo*
U.S. Army Aviation Development Directorate
Aviation and Missile Research
Development and Engineering Center
Research, Development, and Engineering Command
Ames Research Center, Moffett Field, CA

Jeffrey Bosworth
Rotor Dynamics
Bell Helicopter
Textron, Inc.
Fort Worth, TX

C. W. Acree, Jr.
Aeromechanics Office
National Aeronautics and
Space Administration
Ames Research Center
Moffett Field, CA

Andrew R. Kreshock
U.S. Army Research Laboratory
Vehicle Technology Directorate
Hampton, VA

Tiltrotor whirl flutter in cruise flight is investigated using comprehensive rotorcraft analysis codes Comprehensive Analytical Model of Rotorcraft Aerodynamics and Dynamics (CAMRAD) II and Rotorcraft Comprehensive Analysis System (RCAS). A generic tiltrotor model with a three-bladed gimballed rotor was systematically developed starting with a simple rigid rotor mounted on a rigid pylon and a more sophisticated model was built up by adding one design variable at a time. The rotor is also coupled with a flexible wing/pylon modeled from NASTRAN for aeroelastic stability analysis. The effects of pitch–flap coupling (δ_3), blade elasticity, precone, undersling, yoke chord and flap stiffness, pitch link stiffness, rotor rotational speed, density, speed of sound, inflow modeling, unsteady aerodynamics, and realistic airfoil tables on whirl flutter speed are thoroughly examined. With careful and thorough modeling/analysis, aeroelastic stability (frequency and damping) calculated by CAMRAD II and RCAS shows consistently excellent agreement with each other for wide variations of design variables and operating conditions. For the configurations investigated in this study, blade pitch–flap coupling, rotor lag frequency, rotor rotational speed, and density have an important influence on whirl flutter speed.

Nomenclature

a	speed of sound
k_x, k_y, k_z	pitch bearing translational stiffness
$k_{\theta_x}, k_{\theta_y}, k_{\theta_z}$	pitch bearing rotational stiffness
R	blade radius
V	speed
X, Y, Z	translational NASTRAN mode shape at rotor hub
β	flap angle
$\Delta\theta$	blade pitch angle
δ_3	pitch–flap coupling
$\theta_X, \theta_Y, \theta_Z$	rotational NASTRAN mode shape at rotor hub
ν_ζ	blade fundamental lag mode frequency
ρ	freestream density
Ω	rotor rotational speed

Introduction

Aeroelastic instability, specifically whirl flutter, at high-speed airplane mode is a major concern for successful design of future tiltrotor aircraft. A major risk mitigation step for aeroelastic instability in the design and development of tiltrotors is the use of modeling and simulation analyses to ensure adequate speed margins. The principal factor of whirl mode instability is inplane forces of the proprotors coupled with a flexible wing/pylon structure. Considerable experimental and analytical research has been conducted on tiltrotor whirl flutter (Refs. 1–16). To accurately model a sophisticated tiltrotor system, comprehensive rotorcraft analysis codes and multibody dynamics codes have been used to understand fundamental mechanisms and correlate with available test data (Refs. 17–22). The validation of analytical methods has met with only limited success. The current analytical tools are not always able to accurately capture changes in the whirl flutter boundary caused by parametric variations. Moreover, significant differences are observed among the analytical tools used. This raises questions about the validity of the current state-of-the-art modeling and simulation tools for the prediction of tiltrotor whirl flutter.

The failure of comprehensive rotorcraft analysis and multibody dynamics codes to consistently match each other's predictions for the WRATS (Wing and Rotor Aeroelastic Test System) model (Refs. 17–22) is a major incentive for the current effort. The WRATS is a 1/5-scale semispan aeroelastic model of the Joint Services Advanced Vertical Lift Aircraft (JVX), which evolved into the V-22 tiltrotor. The WRATS was tested in the Langley Transonic Dynamics Tunnel (TDT). There have been a number of WRATS tests conducted at the TDT that explored different configurations (Refs. 13, 16, 23, 24).

*Corresponding author; email: hyeonsoo.yeo.civ@mail.mil.
Presented at the American Helicopter Society 73rd Annual Forum, Fort Worth, TX, May 9–11, 2017. Manuscript received May 2017; accepted November 2017.

A study began recently to ensure that widely used comprehensive rotorcraft analysis tools, Comprehensive Analytical Model of Rotorcraft Aerodynamics and Dynamics (CAMRAD) II (Ref. 25) and Rotorcraft Comprehensive Analysis System (RCAS) (Ref. 26), provide similar agreement for a representative tiltrotor model with reasonable variations of design values and operating conditions. The most logical way to achieve this objective is to start with a very simplified model, such as a gimballed rotor with rigid blades mounted on a rigid mast with a rotational spring allowing pitch motion, and then build up by adding one design variable at a time. The most sophisticated model developed in this study generally resembles, but is not identical to, the WRATS so that lessons learned from this study can be easily applied to analytical studies of the WRATS.

In this study, a wide range of design parameters are varied and the effects on whirl flutter speed are examined. Emphasis is placed on a systematic investigation of various structural and aerodynamic parameters on tiltrotor whirl flutter and a physical interpretation of the results. This study examines the effects of pitch–flap coupling (δ_3), blade elasticity, yoke chord and flap stiffness, pitch link stiffness, rotor rotational speed, density, and speed of sound on aeroelastic stability.

Much of the existing whirl flutter data and analyses are proprietary and cannot be openly shared; thus many researchers who develop their own analysis tools have limited opportunities to assess their validity. The research reported here is completely in the public domain and is structured to include a careful buildup in complexity to ensure traceability of model features and analytical methods. All of the geometric and material properties are documented so that any researchers who are interested in tiltrotor whirl flutter analysis can reproduce our results.

In summary, the purpose of this paper is threefold: (1) to compare the comprehensive analysis codes CAMRAD II and RCAS and assess how well their whirl flutter predictions match for generic tiltrotor configurations, (2) to systematically explore a wide range of design parameters and examine their effects on whirl flutter speed, and (3) to report complete information on the present model features, analysis methods, and aeroelastic stability results that can provide a benchmark for researchers who are unable to access proprietary data for the evaluation of their in-house analysis tools.

Description of Analytical Methods

The comprehensive rotorcraft analysis codes CAMRAD II and RCAS are used for modeling and analysis of generic tiltrotor configurations with a gimballed hub. This section provides brief summaries of the two codes and then describes how they are used for whirl flutter analysis in cruise in this study. Similarities and differences between the two modeling and analysis methods are emphasized.

Overview of CAMRAD II and RCAS

CAMRAD II is an aeromechanics analysis of rotorcraft that incorporates a combination of advanced technologies including multibody dynamics, nonlinear finite elements, and rotorcraft aerodynamics. The mathematical model allows structural, aerodynamic, and kinematic nonlinearities and arbitrarily large motion, including rigid body motions and large rotations of components. Thus, CAMRAD II can model the true geometry of a rotorcraft, including multiple load paths such as control systems, lag dampers, tension/torsion straps, and bearingless rotors.

The aerodynamics of CAMRAD II uses a lifting line approach based on airfoil lookup tables combined with an inflow model. Three models for the unsteady aerodynamic loads in attached flow are implemented: incompressible thin airfoil theory (Ref. 27), ONERA EDLIN (Ref. 28), and Leishman–Beddoes (Ref. 29). Five semiempirical dynamic stall models are available in CAMRAD II. Details of the aerodynamic models implemented in CAMRAD II can be found in Ref. 30.

For steady-state loads, CAMRAD II calculates periodic response using a harmonic balance method or time finite element method. An iterative procedure is used to calculate trim settings. CAMRAD II has been used to study tiltrotor performance and loads (Ref. 31) and aeroelastic stability characteristics (Refs. 10, 11).

RCAS is a comprehensive multidisciplinary software system for predicting rotorcraft aerodynamics, performance, stability and control, aeroelastic stability, loads, and vibration. RCAS is capable of modeling a wide range of complex rotorcraft configurations operating in hover, forward flight, and maneuvering conditions. The RCAS structural model employs a hierarchical, finite element, multibody dynamics formulation for coupled rotor–body systems. It includes a library of primitive elements including nonlinear beams, rigid body mass, rigid bar, spring, damper, hinges and slides to build arbitrarily complex models.

The aerodynamics of RCAS uses a lifting line approach based on airfoil lookup tables combined with an inflow model. Unsteady airloads are based on several linear and nonlinear modeling options. Linear unsteady airloads include classical Theodorsen theory (Ref. 32) and a finite state airfoil theory of Peters et al. (Ref. 33). Nonlinear unsteady modeling includes the ONERA (Ref. 28) and Leishman–Beddoes (Ref. 29) models with options for dynamic stall, unsteady trailing edge separation effects, vortex shedding, and yawed flow effects. Reference 34 describes the various modeling options available in RCAS.

In RCAS, the nonlinear equations are solved by direct time domain integration for trim and maneuver problems. A harmonic balance method is also available for trim analysis. RCAS has been used recently for performance, loads, and stability analyses of various rotors (Refs. 35–37).

Common modeling and analysis features of CAMRAD II and RCAS

CAMRAD II and RCAS have similar aerodynamic models. Each rotor blade is modeled with a number of spanwise aerodynamic panels, considered to act as two-dimensional (2D) airfoils. Local velocity components determine the local section angle of attack and Mach number. The lift, drag, and pitching moment on each panel are calculated using airfoil characteristics from C81 lookup tables. Both codes provide a variety of options for corrections to 2D aerodynamics, including swept and yawed flow, spanwise drag, Reynolds number corrections, and unsteady airloads. Only the last of these were studied for this paper, on the grounds that unsteady effects are the most important for aeroelastic stability over the operating conditions examined. Dynamic stall effects are not relevant for a proprotor operating in its design range and were therefore ignored.

CAMRAD II and RCAS have complete multibody dynamics models of the hub and control system, including gimbal, pitch bearings, pitch links, and all associate joints. Control system stiffness is included. Both codes model the blade structure as a series of nonlinear beam elements, optionally with multiple load paths. The effects of rigid, elastic, single-load path, and dual-load path models are examined in this paper.

Both analyses model the airframe dynamics as an orthogonal modal model, with frequencies and mode shapes generated by an external code, NASTRAN. In addition, both codes can optionally model the airframe as a simple mass-spring-damper system, here representing a rigid pylon attached to the wing with a hinge and spring. Both types of airframe model are explored here.

For airplane-mode aeroelastic stability wind tunnel testing, the rotor system is normally operated in windmill state (zero torque) because this state represents the most conservative manner to test the stability of the system. For the analytical results presented in the current paper, the rotor is first trimmed to zero torque at a given wind velocity and tip speed.

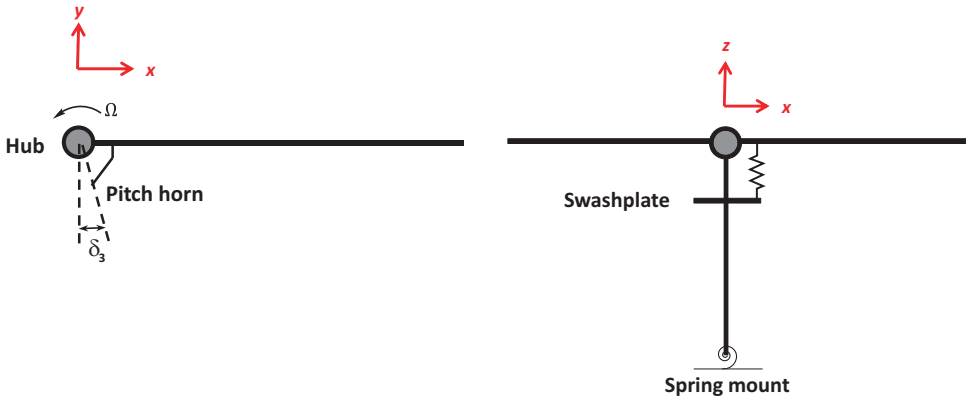

(a) Front view (b) Top view

Fig. 1. Generic tiltrotor front and top view in airplane mode.

Once the rotor is trimmed to a specified operating condition, CAMRAD II and RCAS linearize the equations about the trim solution and calculate frequency and damping using a constant-coefficient approximation. A constant-coefficient approximation is suitable for axial flow conditions. The Floquet method, which solves periodic equations, was applied to the baseline model and produced results identical to the constant-coefficient approximation. Only constant-coefficient analyses are shown here. A 30° (12 steps per rotor revolution) azimuthal step size was used to average the stability matrices for both CAMRAD II and RCAS analyses. To compute coupled rotor/airframe aeroelasticity, both trim and stability analyses are carried out in the fixed frame by transforming rotor blade equations to the fixed frame using multiblade coordinate transformation.

Different modeling and analysis features of CAMRAD II and RCAS

In the present CAMRAD II analysis, trim analysis was conducted using harmonic balance and a single steady (constant) harmonic, which was computationally efficient and appropriate for a cruise condition. For stability analysis, five harmonics were used. A 15° (24 steps per rotor revolution) azimuthal step size was used for the trim calculations. For an elastic rotor analysis, a modal reduction approach was used to reduce the number of degrees of freedom from a large system of equations.

Although a modal analysis method is available, the current RCAS analysis maintained full finite element representation of the rotor throughout the dynamic analysis and did not use harmonic truncation. A 5.0° (72 steps per rotor revolution) azimuthal step size was used for the trim calculations.

Both codes have a variety of inflow models, from a simple uniform inflow model to a sophisticated free-wake model. Uniform inflow is completely adequate for high-speed axial flow, because the induced velocity is a very small fraction of the total inflow. For both trim and stability analyses, CAMRAD II used the uniform inflow model to include induced velocity and RCAS used two inflow options, with and without induced velocity, but only results without induced velocity effects are presented. As will be shown, the results are essentially identical.

In the present CAMRAD II analysis, an elastic rotor was modeled using 11 nonlinear beam elements (three elements for yoke, one element for cuff, and seven elements for blade) and 17 aerodynamic panels. The solution for the trim and stability analyses used six elastic blade modes plus gimbal degrees of freedom. In the RCAS analysis, an elastic rotor was modeled using 12 nonlinear beam elements (four elements for yoke, three elements for cuff, and five elements for blade) and 17 aerodynamic segments.

Results and Discussion

Comparisons between CAMRAD II and RCAS stability analyses are conducted systematically for various problems, and the calculated results are presented. This section consists of three subsections: (1) rigid rotor analyses, (2) elastic rotor analyses, and (3) parametric studies. The analyses started with a rigid rotor mounted on a rigid mast and then built up by adding one design variable at a time. A wide range of design parameters are varied, and the effects on whirl flutter speed are examined.

Rigid rotor analyses

As shown in Figs. 1 and 2, the first case used a three-bladed gimballed rotor with 4-ft radius and −40° twist rate mounted on a 4-ft rigid mast with 84,000 inch-lb/rad pitch spring at the bottom. This is a single load-path model with a single pitch bearing with stiffness value of 57.296 inch-lb/rad at 2.5 inches spanwise. The properties needed to model and analyze this initial generic rotor are provided in Table 1. Pitch–flap coupling (δ_3) is introduced by the control system geometry as shown in Fig. 1(a). When the pitch bearing is outboard of the (effective) flap hinge, the blade experiences a pitch change due to flapping if the pitch link is not in line with the flapping axis. Pitch–flap coupling causes a pitch change when the blade flaps according to the relationship, $\Delta\theta = (-\tan\delta_3)\beta$. Negative δ_3 produces positive pitch–flap coupling, which means the blade pitch increases with an increase in flap angle. Negative δ_3 is commonly

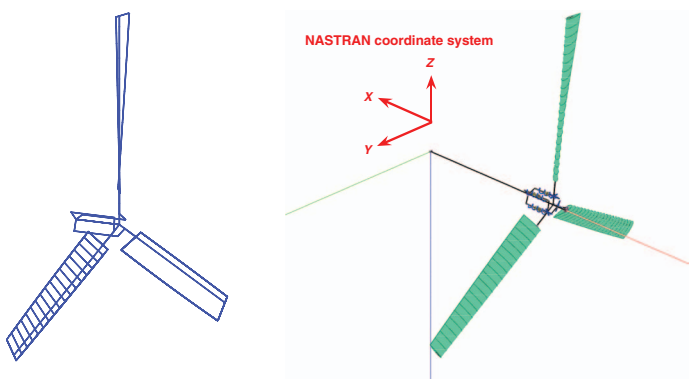

(a) CAMRAD II (b) RCAS

Fig. 2. CAMRAD II and RCAS generic tiltrotor model in airplane mode.

Table 1. Description of the initial generic rotor model

Rotor	
Type	Gimballed
Number of blades	3
Rotational speed, RPM	742
Blade radius, inches	48
Blade chord, inches	6
Blade twist rate, deg	−40, linear
Blade twist at 75% span, deg	15
Blade tip speed, inch/s	3730
Blade tip Mach number	0.28
Yoke and cuff twist, deg	0
Blade weight per length, lb/inch	0.06
Total rotor weight, lb	8.64
Gimbal spring stiffness, inch-lb/rad	25
Pitch link stiffness, lb/inch	975
δ_3, deg	−15
Precone, deg	0
Undersling, inch	0
Structural damping, %	1.0
Lift curve slope, /rad	5.7
Drag coefficient	0.0095
Moment coefficient	0.0
Pylon	
Mast length, inches	48
Weight per length, lb/inch	0.01
Spring stiffness, inch-lb/rad	84,000
Damping, inch-lb-s/rad	104.4

used for tiltrotor design because it increases the blade flap–lag stability and effectively reduces steady-state and transient flapping (Ref. 3). For the current model shown in Fig. 1, the pitch link attaches on the trailing edge side. The pitch link attachment to pitch horn is located at 0.7 inch spanwise and 2.6 inches chordwise relative to the hub origin. The pitch horn attachment to the blade is at 2.5 inches spanwise. The pitch link attachment to swashplate is located 12 inches below the hub plane. Pitch link stiffness value is 975 lb/inch.

The model operates in a free-stream velocity (V) with the shaft always parallel to the free stream so that the rotor equilibrium flow is purely axial. Operating conditions are sea level standard and 742 RPM rotor speed. Both CAMRAD II and RCAS modeled each baseline blade as rigid. The airloads are modeled with linear airfoil aerodynamics: airfoil lift curve slope of 5.7, drag coefficient of 0.0095, and zero pitching moment. The airfoils were aligned with the blade structural twist. Effects of compressibility, unsteady aerodynamics, and static/dynamic stall are ignored. Again, CAMRAD II used uniform induced inflow, whereas RCAS did not include induced velocity. Both CAMRAD II and RCAS analyses used 17 aerodynamic segments. The rotor is trimmed to zero torque to simulate a windmilling condition.

Table 2. Bearing locations and stiffness values

	Inner bearing	Outer bearing
Station, inches	2.5	7.5
k_x, lb/inch	0	infinite
k_y, lb/inch	90,000	90,000
k_z, lb/inch	90,000	90,000
k_{θ_x}, inch-lb/rad	57.296	57.296
k_{θ_y}, inch-lb/rad	57.296	57.296
k_{θ_z}, inch-lb/rad	57.296	57.296

Figure 3 shows frequency and damping values of the pylon pitch mode as a function of velocity, with four different values of pitch–flap coupling (δ_3). The speed range was 30–150 kt, with trim and stability calculated in 10-kt increments. For the δ_3 variation, both pitch link top and bottom points are rotated with respect to the shaft axis. The rotor in airplane mode was first trimmed to zero torque with collective. The CAMRAD II analysis used harmonic balance, and the RCAS used direct time domain integration. Then, the stability analysis linearized the equations about the trim solution and calculated frequency and damping using constant-coefficient equations. Positive damping indicates a stable system, and negative damping indicates instability. As expected, an increase in pitch–flap coupling is destabilizing. Whirl flutter speed was reduced from about 120 kt with $\delta_3 = -15^\circ$ to about 50 kt with $\delta_3 = -45^\circ$. There is excellent agreement between the two analyses in both frequency and damping.

In the second case, an outboard bearing was added to model a dual load-path rotor with separate yoke and cuff structural elements. The inboard and outboard bearing locations and stiffness values are presented in Table 2. Blade pitch control moments are applied to the cuff through a conventional swashplate/pitch link/pitch horn system. The pitch horn is attached to the cuff at 2.5 inches spanwise. The inboard bearing is free

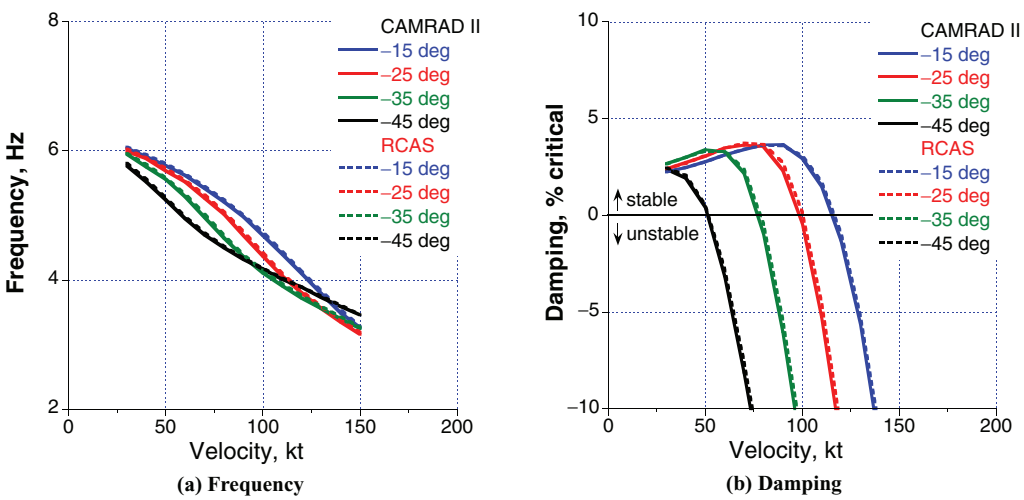

Fig. 3. Effects of δ_3 on frequency and damping of pylon pitch mode for single load-path configuration.

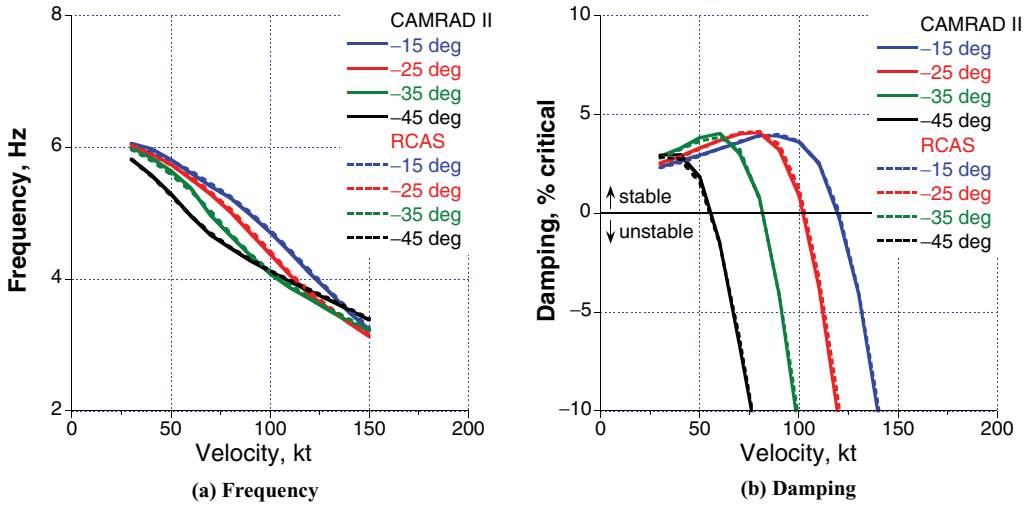

(a) Frequency (b) Damping

Fig. 4. Effects of δ_3 on frequency and damping for dual load-path configuration.

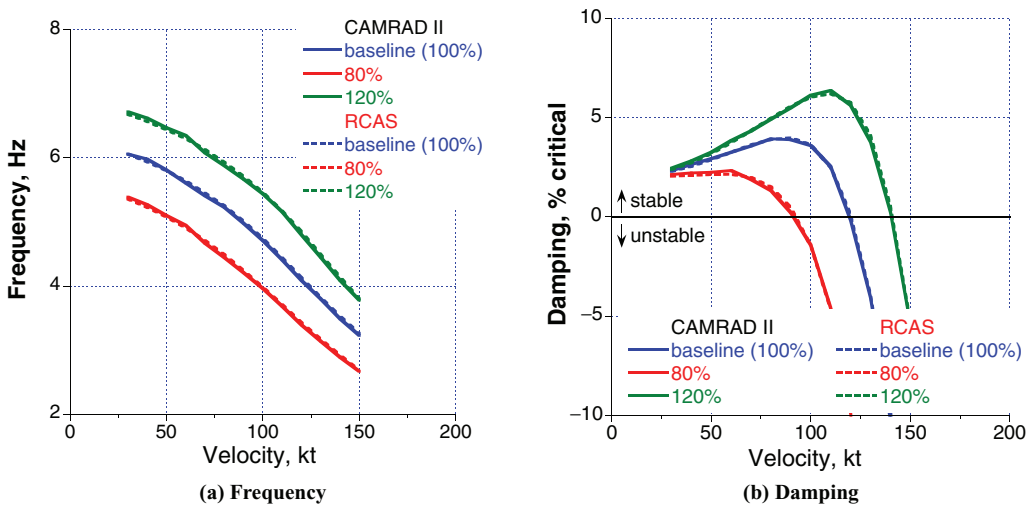

(a) Frequency (b) Damping

Fig. 5. Effects of pylon stiffness on frequency and damping of pylon pitch mode for dual load-path configuration.

Table 3. NASTRAN wing/pylon frequencies and mode shapes at the rotor hub

Mode	Frequency (Hz)	X (inches)	Y (inches)	Z (inches)	θ_X (rad)	θ_Y (rad)	θ_Z (rad)
Wing beam	3.43	0.000	0.000	−2.673	−0.025	−0.015	0.000
Wing chord	6.83	−2.024	−1.593	0.000	0.000	0.000	0.033
Wing torsion	8.63	0.000	0.000	3.954	−0.020	0.116	0.000
Pylon yaw	14.67	−0.720	4.480	0.000	0.000	0.000	−0.093

to move axially, and the cuff does not carry centrifugal force. For areas of dual load path (yoke and cuff), 0.03 lb/inch mass was allocated to each so that the total rotor mass is same as the single load-path model. Frequency and damping values of the pylon pitch mode are plotted in Fig. 4 with four different values of pitch–flap coupling (δ_3). Because the rotor blade is rigid, the whirl flutter boundary did not change much compared to the first case (single load path). Again, there is excellent agreement between the two analyses in both frequency and damping.

Effects of pylon stiffness are examined in Fig. 5 for the dual load-path configuration with $\delta_3 = -15^\circ$. A 20% variation of the pylon stiffness from the baseline value (84,000 inch-lb/rad) changed the frequency of the pylon mode by 11% at 30 kt and 17% at 150 kt. Pylon stiffness has a very small influence on damping at 30 kt. However, it has an important role as speed increases. A 20% increase of pylon stiffness increased whirl flutter speed by about 20 kt, and a 20% decrease of pylon stiffness reduced whirl flutter speed by about 30 kt. The peak damping value also significantly changed with varying pylon stiffness. A 20% increase of pylon stiffness increased the peak damping to 6.4% from about 4% for the baseline.

Next, the one-degree-of-freedom rigid mast was replaced with a flexible wing/pylon modeled in NASTRAN. The wing root is attached to a fixed support with cantilever root restraint. A pylon with large mass and moment of inertia is rigidly attached to the wing tip, and a lumped mass of 8.64 lb is included to represent the rotor. Table 3 shows the

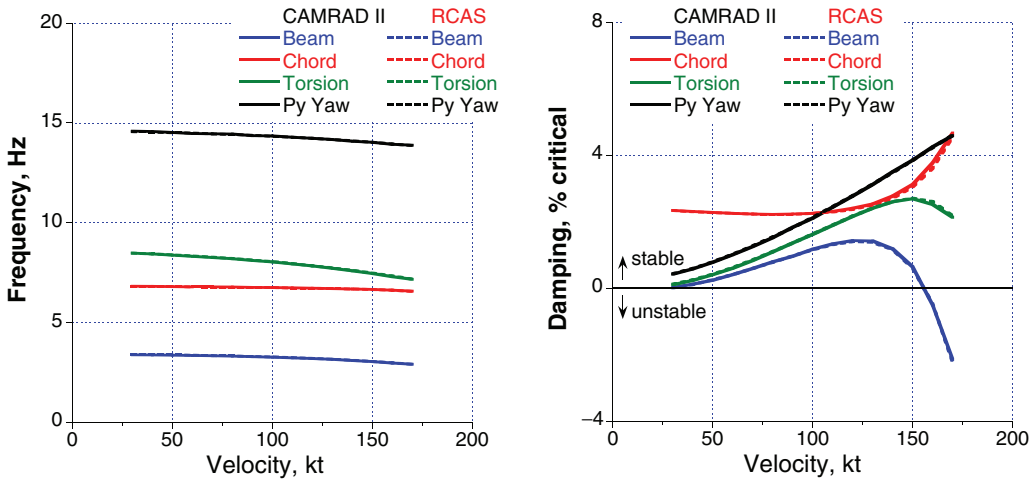

(a) Frequency (b) Damping

Fig. 6. Frequency and damping of wing/pylon modes for rigid rotor configuration.

Table 4. Elastic rotor properties

Yoke flap stiffness at 0 inch, lb-inch^2	36,000
Yoke flap stiffness at 7.5 inches, lb-inch^2	5040
Yoke chord stiffness at 0 inch, lb-inch^2	288,000
Yoke chord stiffness at 7.5 inches, lb-inch^2	100,800
Yoke torsional stiffness, lb-inch^2	1.008×10^7, uniform
Cuff flap stiffness, lb-inch^2	1.728×10^6, uniform
Cuff chord stiffness, lb-inch^2	1.728×10^6, uniform
Cuff torsional stiffness, lb-inch^2	1.008×10^9, uniform
Blade flap stiffness, lb-inch^2	1.44×10^7, uniform
Blade chord stiffness, lb-inch^2	1.44×10^7, uniform
Blade torsional stiffness, lb-inch^2	1.008×10^9, uniform
Section flap moment of inertia, lb-s^2	1.1×10^{-5}, uniform
Section chord moment of inertia, lb-s^2	2.0×10^{-4}, uniform
Pitch link stiffness, lb/inch	558.33

wing/pylon modal characteristics normalized to unit-generalized mass. The calculated modes included wing out-of-plane bending (beam mode), inplane bending (chord mode), torsion, and pylon yaw. The coordinate system (NASTRAN) is right-handed in translation and rotation as shown in Fig. 2(b): $+X$ aft, $+Y$ outboard, and $+Z$ up. Note that wind direction is $+X$ and the hub out-of-plane direction is $-X$. The mode shape output is at the hub. Structural damping values can be accounted for in either CAMRAD II or RCAS, but zero wing structural damping and zero wing aerodynamic damping are assumed for the present analyses. The wing/pylon NASTRAN modes are coupled with the rigid rotor model. Figure 6 shows frequency and damping values of the various wing/pylon modes. The results show that the wing-beam mode (lowest frequency mode) is the primary participant of whirl flutter, with a whirl flutter speed of 155 kt. The other modes are highly damped for the speed range examined.

Elastic rotor analyses

In this subsection, a rigid rotor approximation is removed and an elastic rotor is used for the aeroelastic stability analysis. Elastic rotor properties are provided in Table 4. Mass of the elastic rotor remains same as that of the rigid rotor. Yoke flap and chord stiffnesses are linearly distributed along the span, whereas yoke torsion and cuff and blade flap, chord, and torsion stiffnesses are constant. Pitch link stiffness is reduced to 558.33 lb/inch from 975 lb/inch for the rigid blade model.

In the CAMRAD II analysis, the elastic rotor was modeled using 11 nonlinear beam elements (three elements for yoke, one element for cuff, and seven elements for blade) and 17 aerodynamic panels. The solution for the trim and stability analyses used six elastic blade modes (three flap, two lag, and one torsion mode) plus gimbal degrees of freedom. In the RCAS analysis, the elastic rotor was modeled using 12 nonlinear beam elements (four elements for yoke, three elements for cuff, and five elements for blade) and 17 aerodynamic segments. The RCAS analysis maintained full finite element representation of the rotor without modal reduction. It will be shown that the stability results are essentially identical even with these differences, which means a sufficient number of elements are used in the current analyses. Both CAMRAD II and RCAS models with nine nonlinear beam elements (three elements for yoke, one element for cuff, and five elements for blade) exactly reproduced the results shown here.

Figure 7 shows frequency and damping values of the various wing/pylon modes with $\delta_3 = -15^\circ$. The speed range was 30–200 kt, with trim and stability calculated in 10-kt increments. When the wing/pylon NASTRAN modes were coupled with the elastic rotor model, the frequencies did not change much (compare Figs. 6(a) and 7(a)), but the resulting whirl flutter speed was higher than for the rigid rotor (compare Figs. 6(b) and 7(b)). Whirl flutter speed increased from 155 to 185 kt. This increased whirl flutter speed is primarily attributed to the elastic inplane mode. There is excellent agreement between the CAMRAD II and RCAS analyses in both frequency and damping. One interesting point is the increase in damping at 50 kt. The wing beam mode and the blade regressive lag mode (ν_ζ -1/rev) cross at that speed as shown in Fig. 7(c). The peak damping occurs where the frequencies of the blade regressive lag mode and wing beam mode cross; hence, it is an effect of the coupling of the rotor lag and wing-bending modes. The regressive lag mode damping keeps increasing, and the wing beam mode damping decreases with speed as shown in Fig. 7(d). The rotor lag motion has a very important influence on the wing modes, especially the wing beam mode damping. Further analysis is conducted in the section "Parametric studies." Frequencies of the principal rotor modes are also plotted along with the wing mode frequencies in Fig. 8 to better understand the dynamic characteristics of the coupled rotor/wing system. There is excellent agreement between the CAMRAD II and RCAS analyses for all rotor mode frequencies.

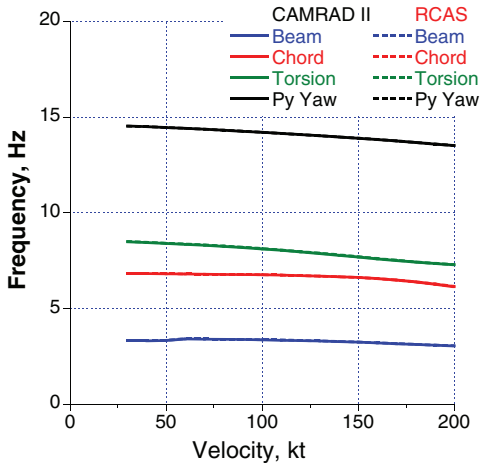

(a) Frequency

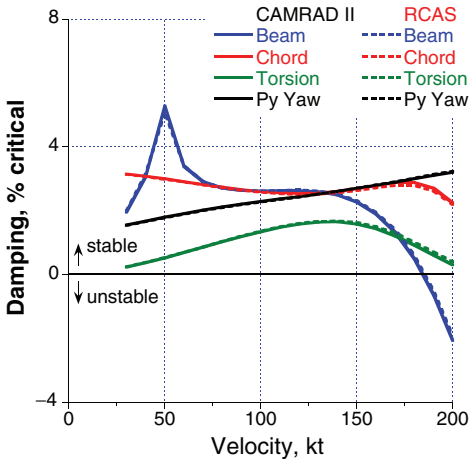

(b) Damping

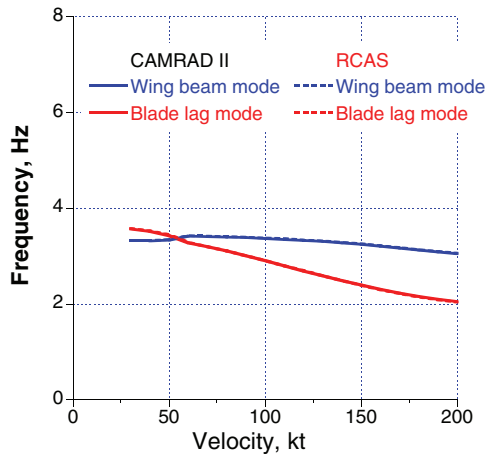

(c) Frequency variation of wing beam and blade lag modes

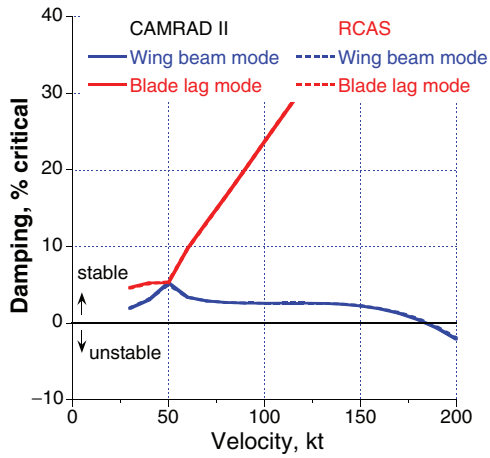

(d) Damping variation of wing beam and blade lag modes

Fig. 7. Frequency and damping of wing/pylon modes for elastic rotor configuration.

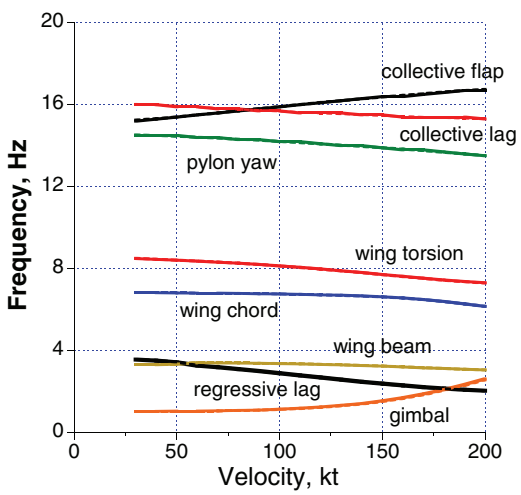

Fig. 8. Frequency of rotor and wing modes for elastic rotor configuration (solid lines are CAMRAD II and dotted lines are RCAS results).

Up to this point, unsteady aerodynamics, compressibility, and stall effects were ignored in the analyses. These effects are sequentially added to the model with an elastic rotor and wing/pylon NASTRAN modes. Figure 9 shows the effects of unsteady aerodynamics on aeroelastic stability. Unsteady lift and moment in attached flow are calculated based on thin airfoil theory. The CAMRAD II analysis used an unsteady model based on incompressible thin airfoil theory. RCAS used linear unsteady airloads based on classical Theodorsen theory. Unsteady aerodynamics reduces whirl flutter speed from 185 to 177 kt. There is excellent agreement between the CAMRAD II and RCAS analyses in both frequency and damping. Although not shown here, CAMRAD II analysis has also been conducted with the ONERA EDLIN model, which approximates compressible thin airfoil theory. There was a negligible change in damping with the ONERA EDLIN model, and thus whirl flutter speed did not change.

To include realistic blade section aerodynamics such as compressibility and stall, four airfoils from the XV-15 tiltrotor are added to both models. Section lift, drag, and moment values for the airfoils are obtained from lookup tables provided in Appendix A of Ref. 10. The four airfoils are distributed along the blade span. Using the same naming convention as in Ref. 10, the first airfoil is located at radial stations of $0.15625R$ (root cutout) $-$ $0.55R$, the second airfoil at $0.55R - 0.8R$, the third airfoil at $0.8R - 0.95R$, and the fourth airfoil at $0.95R - 1.0R$. Figure 10 shows the effects of using airfoil tables (and thus compressibility and stall effects). Unsteady aerodynamics is also included in this analysis. In general, nonlinear aerodynamics slightly reduces whirl flutter speed to 174 kt, but its effect is small.

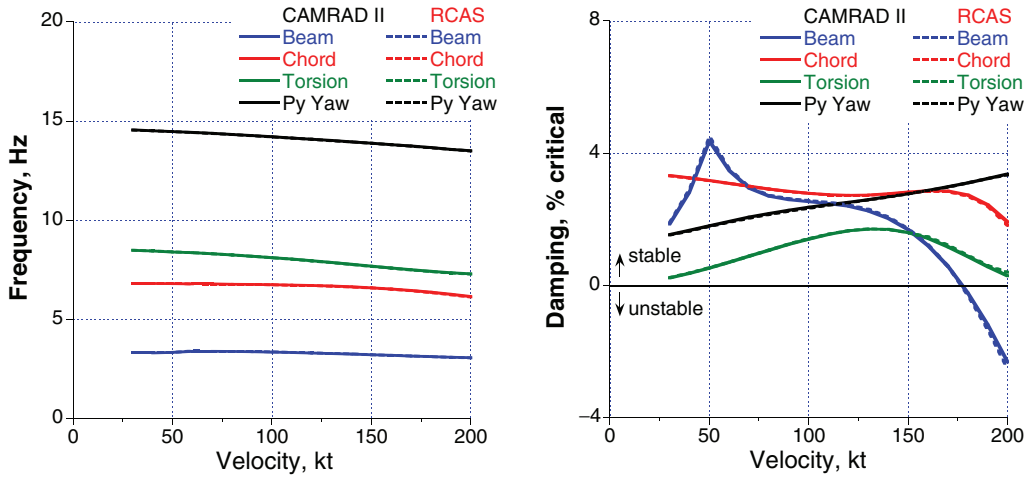

(a) Frequency (b) Damping

Fig. 9. Frequency and damping of wing/pylon modes for elastic rotor with unsteady aerodynamics configuration.

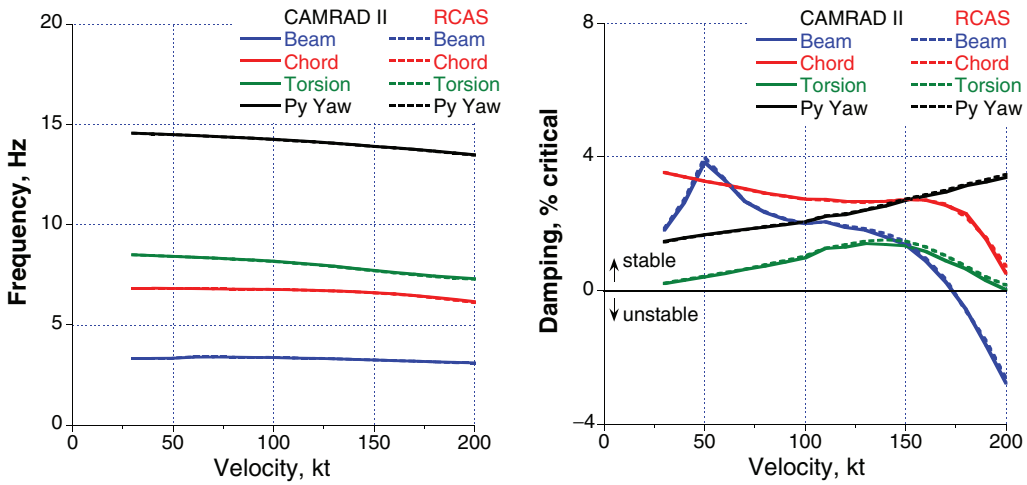

(a) Frequency (b) Damping

Fig. 10. Frequency and damping of wing/pylon modes for elastic rotor with XV-15 airfoil configuration.

For tiltrotor aircraft such as XV-15 and V-22, the hub is gimballed with underslung. In an underslung system, the rotor blades lie in a plane below the plane containing the rotor hub pivot point. Because of coning, normal rotor operating RPM will place the center of mass of the rotor blades in approximately the same plane as the rotor hub pivot point. Precone is usually employed to relieve the root-bending stresses that arise from the steady flap bending moment. Underslung and precone are sequentially included in the rotor model, and their effects on aeroelastic stability are examined.

Figure 11 shows the influence of underslung (and overslung) on aeroelastic stability. The model used for this analysis includes both unsteady aerodynamics and XV-15 airfoil tables. A δ_3 of -15° and precone of 0° are used. The wing beam mode frequency and damping values are compared for the baseline (no underslung), $-4\%R$ and $-2\%R$ underslung, and $+2\%R$ and $+4\%R$ overslung configurations. Wing beam frequencies did not change much at low speeds, but overslung increases wing beam frequencies and underslung decreases wing beam frequencies at high speeds. Underslung increases damping at high speeds compared to the baseline with no underslung. Whirl flutter speed is increased from 174 to 183 kt with $-2\%R$ underslung and 196 kt with $-4\%R$ underslung. Although overslung slightly reduces damping, it has small influence on whirl flutter speed. Whirl flutter speed is reduced to 169 kt with $+2\%R$ overslung and 168 kt with $+4\%R$ overslung.

Figure 12 shows the influence of precone on aeroelastic stability. The wing beam mode frequency and damping values are compared for precone of 0° (the baseline value), 2.5°, and 5.0°. The model used for this analysis includes $-2\%R$ underslung, -15° δ_3, XV-15 airfoils, and unsteady aerodynamics. A net flap moment acting on the rotor blade in axial flight creates a moment component along the blade pitch axis when the blade lags, and this component should be balanced by control system stiffness. Thus pitch–lag coupling occurs (positive for lag back, pitch down). When the precone is chosen for the high loading condition (e.g., hover) but the rotor in cruise is operating at very low loading, the trim coning angle is negative and this generates negative pitch–lag coupling. Reference 5 showed that this negative pitch–lag coupling due to precone has a destabilizing influence on whirl flutter. Reference 13 showed that, although precone has a destabilizing effect, a flexure hub, which decreases coning angle under centrifugal force, reduces the effects of pitch–lag coupling compared to a rigid hub. The present results show that the negative pitch–lag coupling due to precone reduces whirl flutter

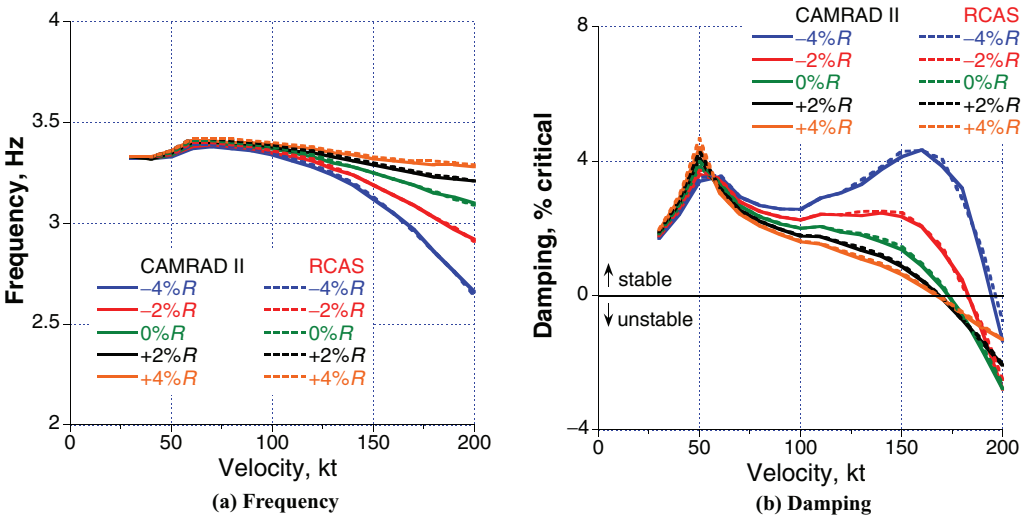

(a) Frequency (b) Damping

Fig. 11. Frequency and damping of wing beam mode for elastic rotor with undersling.

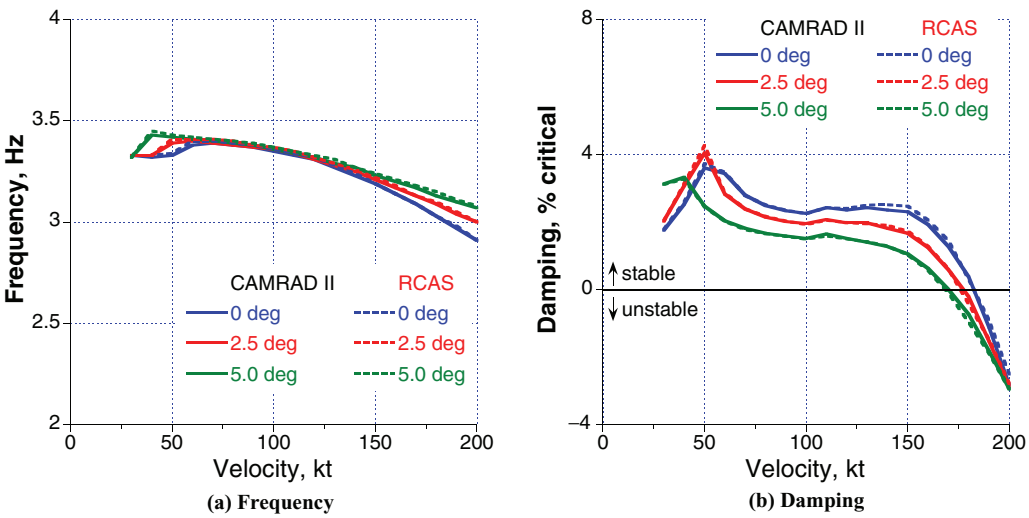

(a) Frequency (b) Damping

Fig. 12. Frequency and damping of wing beam mode for elastic rotor with precone.

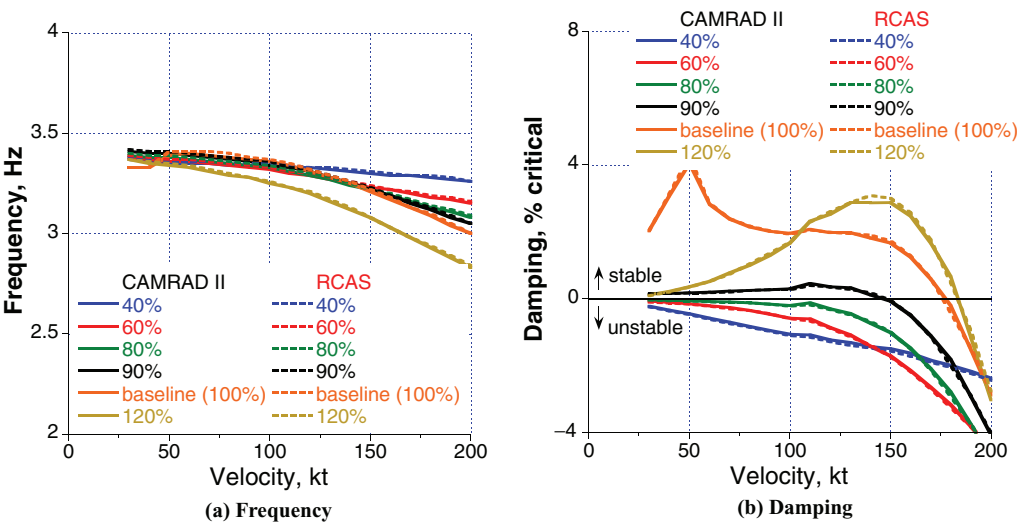

(a) Frequency (b) Damping

Fig. 13. Frequency and damping of wing beam mode with yoke chord stiffness variation.

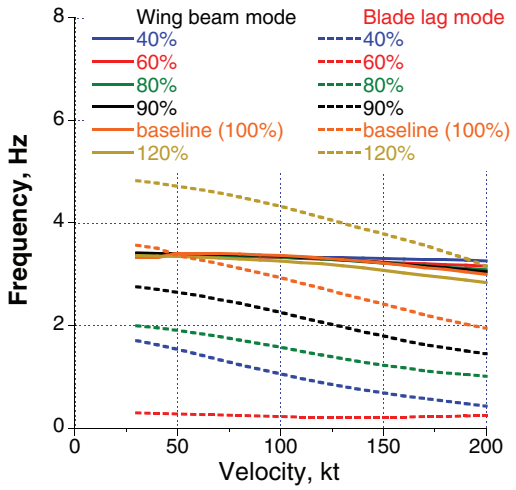

Fig. 14. Comparison between wing beam mode and blade lag mode frequencies with yoke chord stiffness variation (RCAS analysis).

speed, which is consistent with the results in Refs. 5 and 13. Whirl flutter speed is reduced from 183 kt for the baseline (0° precone) to 176 kt for the 2.5° precone and to 169 kt for the 5.0° precone.

Parametric studies

Starting with a simple rigid rotor mounted on a rigid pylon, a more sophisticated model was built up by adding one design variable at a time. The three-bladed gimballed rotor with dual load path, elastic blades, $-2\%R$ undersling, 2.5° precone, $-15°$ δ_3, and XV-15 airfoils includes all the key design parameters of realistic tiltrotor configurations. The rotor is coupled with the flexible wing/pylon modeled from NASTRAN for aeroelastic stability analysis. Parametric studies are conducted in this subsection using this model as a baseline. The parameters investigated in this study are yoke chord and flap stiffness, pitch link stiffness, pitch–flap coupling (δ_3), rotor rotational speed, density, and speed of sound. The effects of those parameters on the wing beam mode frequency and damping are examined.

Figure 13 shows the effects of yoke chord stiffness variation on aeroelastic stability. The yoke chord stiffness values are uniformly varied to 40%, 60%, 80%, 90%, and 120% of the baseline values. The cuff and blade properties remain the same. The rotor lag mode has a very important influence on the wing modes, especially the wing beam mode damping. To better understand the damping changes, blade lag (regressive lag mode) frequencies are also plotted along with the wing beam mode frequencies in Fig. 14. Only RCAS results are plotted in this figure. Blade lag frequencies decrease as the chord stiffness is reduced up to 60% of the baseline value. However, the rotating lag frequency becomes less than 1/rev (soft inplane) when the chord stiffness is further reduced to 40% of the baseline value and then the nonrotating lag frequency increases compared to that for the 60% chord stiffness case. Note that the regressive lag frequency is ν_ζ −1/rev for a stiff inplane rotor and 1/rev $-\nu_\zeta$ for a soft inplane rotor. The decrease in the lag frequency with speed is the effect of reduced stiffness due to increasing blade pitch. Owing to the varied lag frequencies, the frequency crossing between the wing beam mode and the blade regressive lag mode was avoided and thus the wing beam mode damping does not show a peak at 50 kt (Fig. 13(b)). The increased chord stiffness (thus lag frequency) increases damping at high speed and increases whirl flutter speed from the baseline value of 176 kt to 183 kt. The decreased chord stiffness (thus lag frequency) significantly reduces damping, and thus the system is unstable for the entire speed range investigated when the blade chord stiffness was reduced to 80% of the baseline or below.

Figure 15 shows the effects of yoke flap stiffness and pitch link stiffness variation on aeroelastic stability. The yoke flap stiffness values are uniformly varied to 80% and 120% of the baseline values (Fig. 15(a)). The cuff and blade properties remain the same. The pitch link stiffness value is varied by ±20% from the baseline value of 558.33 lb/inch, and the pitch link stiffness value used for the rigid rotor analysis (975 lb/inch) is also included (Fig. 15(b)). Only wing beam damping values are shown as the maximum wing beam frequency change due to the yoke flap stiffness variation and pitch link stiffness variation from the baseline is about 0.04 and 0.01 Hz at 200 kt, respectively. Both reduced flap stiffness and reduced pitch link stiffness increase whirl flutter speed. However, their influence is much smaller than that with the yoke chord stiffness variation. The 20% reduction of yoke flap stiffness increases whirl flutter speed from the baseline value of 176 kt to 180 kt, and the 20% reduction of pitch link stiffness increases whirl flutter speed to 182 kt.

Figure 16 shows the influence of pitch–flap coupling (δ_3) on aeroelastic stability. Wing beam mode frequencies and damping values are plotted with six different values of pitch–flap coupling including zero and

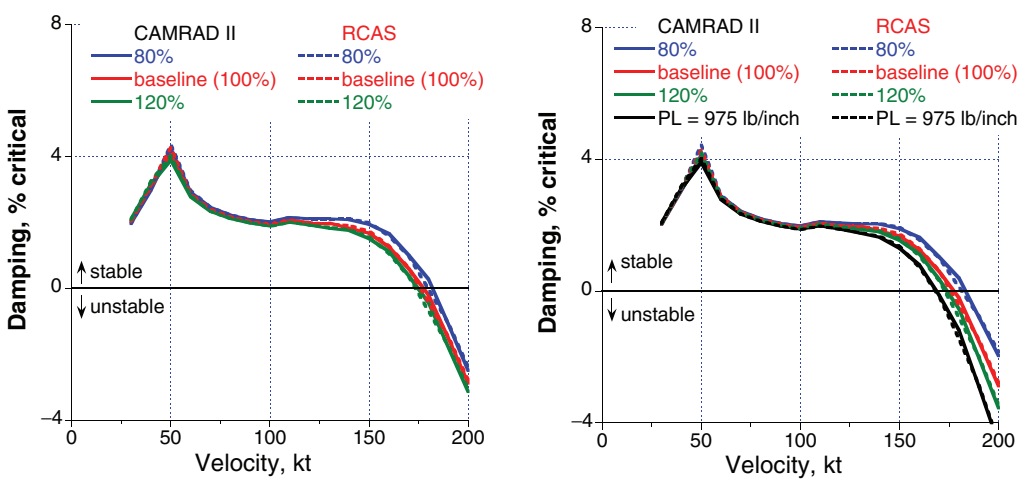

(a) Damping for flap stiffness variation

(b) Damping for pitch link stiffness variation

Fig. 15. Damping of wing beam mode with yoke flap stiffness and pitch link stiffness variation.

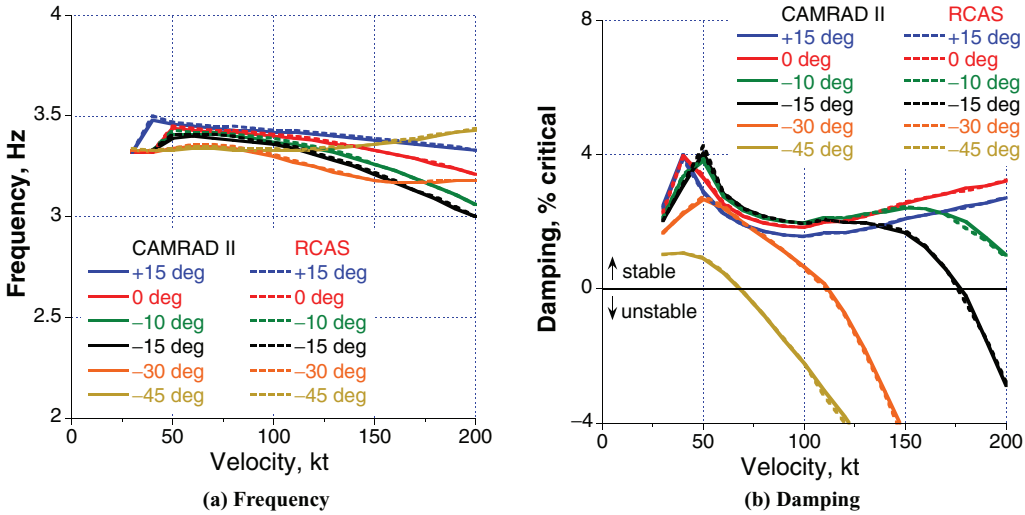

(a) Frequency (b) Damping

Fig. 16. Frequency and damping of wing beam mode with δ_3 variation.

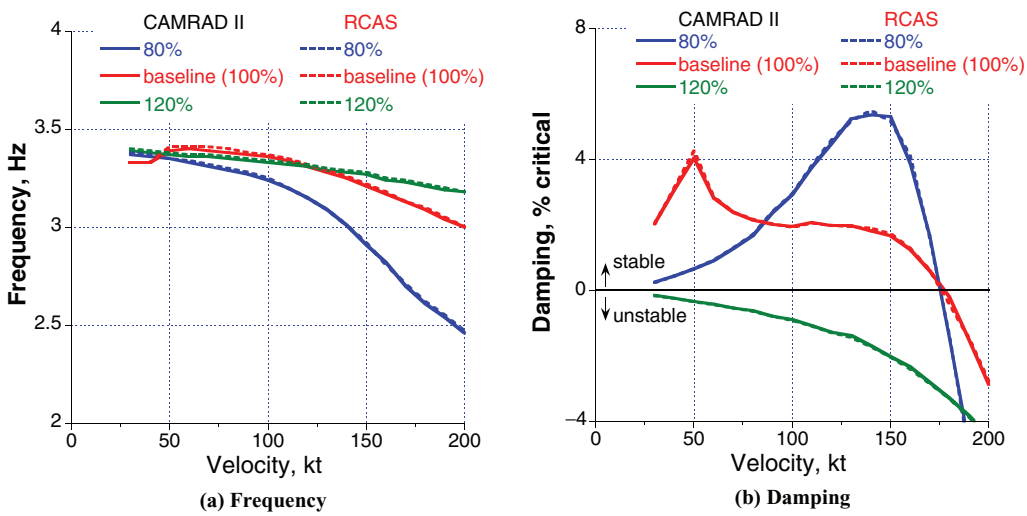

(a) Frequency (b) Damping

Fig. 17. Frequency and damping of wing beam mode with rotor RPM variation.

positive δ_3. Whirl flutter speed is reduced from 176 kt with $\delta_3 = -15^\circ$ to 68 kt with $\delta_3 = -45^\circ$. The damping values are very similar between $\delta_3 = 0^\circ$ and $+15^\circ$, and the wing beam mode is stable for the speed range investigated.

Figure 17 shows the effects of rotor rotational speed on aeroelastic stability. Rotor rotational speed is varied by ±20% from the baseline value of 742 RPM, and the frequency and damping values of the wing beam mode are compared. Variation of rotor rotational speed influences both blade dynamics and aerodynamics by changing blade frequencies, tip Mach number, and centrifugal force. All of these changes affect aeroelasic stability of the system; especially blade lag frequency change appears to have a dominant influence. The decreased rotational speed increases the blade regressive lag mode frequency, and the increased rotational speed decreases the blade regressive lag mode frequency. Thus, rotor rotational speed change has a similar influence on aeroelastic stability as yoke chord stiffness (thus lag frequency). The damping plot for the rotor rotational speed variation (Fig. 17(b)) is similar to that for the yoke chord stiffness variation (Fig. 13(b)). The reduced rotor speed increases a peak damping around 150 kt to more than 4% critical damping. However, it has very small influence on whirl flutter speed. Increased rotor speed makes the system unstable within the speed range investigated.

Figure 18 shows the effects of density and speed of sound on aeroelastic stability. Operating condition for the baseline is sea level standard ($\rho = 0.002377$ slug/ft^3, $a = 1116.5$ ft/s). Density is reduced to 0.001756 slug/ft^3 (density at 10,000 ft altitude) and 0.001267 slug/ft^3 (density at 20,000 ft altitude), which means density is 74% and 53% of the baseline value, respectively. Speed of sound is maintained the same as the sea level value for the density variation. Speed of sound of 700 ft/s is used, which is 63% of the baseline value, to simulate a more realistic Mach number. Density is same as the sea level value for the speed of sound variation. This increases the blade hover tip Mach number from the baseline value of 0.28 to 0.44. As density decreases, damping values increase substantially due to lower dynamic pressure. Eventually, the damping curves come down and become unstable at 222 kt for the 10,000 ft density case and at 288 kt for the 20,000 ft density case (Fig. 19). The decreased speed of sound, and thus increased Mach number, reduces the wing mode damping slightly. In general, it has a small influence on aeroelastic stability. Whirl flutter speed is reduced from 176 to 169 kt.

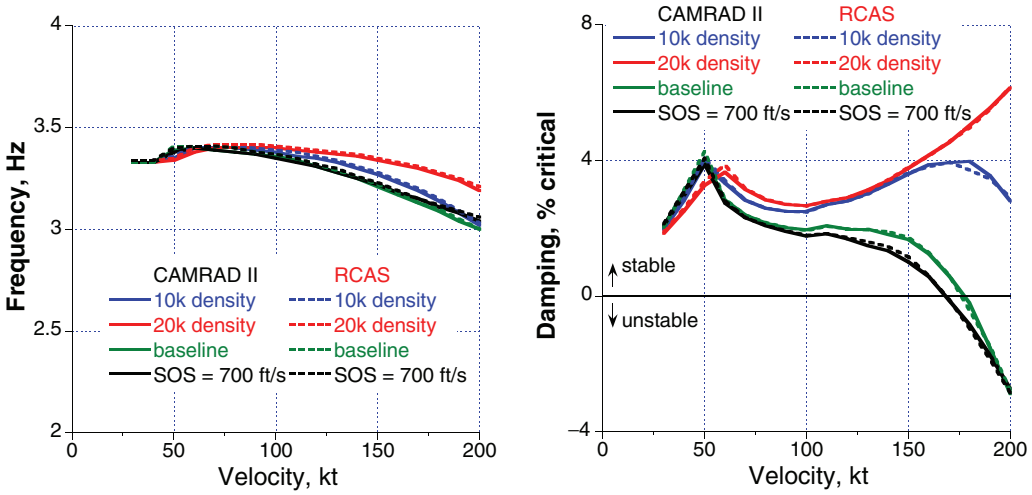

(a) Frequency (b) Damping

Fig. 18. Frequency and damping of wing beam mode with density and speed of sound variation.

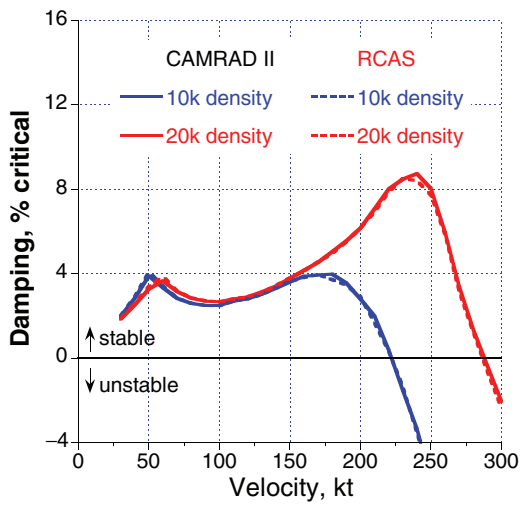

Fig. 19. Damping of wing beam mode with density variation (expanded velocity range).

Conclusions

This paper investigates tiltrotor whirl flutter in cruise flight using comprehensive rotorcraft analysis codes CAMRAD II and RCAS. A generic tiltrotor model with a three-bladed gimballed rotor was systematically developed starting with a simple rigid rotor mounted on a rigid pylon, then a more sophisticated model was built up by adding one design variable at a time. A considerable number of parametric variations were investigated analytically to examine their effects on whirl flutter speed. From this study, the following conclusions are obtained:

1) With very careful and thorough modeling/analysis, frequency and damping values calculated by comprehensive analysis codes CAMRAD II and RCAS show consistently excellent agreement with each other for a representative tiltrotor model with reasonable variations of design values and operating conditions.

2) The blade pitch–flap coupling has an important influence on the aeroelastic behavior of the proprotor. As expected, increased positive pitch–flap coupling (negative δ_3) is destabilizing.

3) The rotor lag mode has a very important influence on the wing beam mode damping. Reducing the yoke chord stiffness (thus regressive lag frequency) significantly decreases damping and thus the system is unstable for the entire speed range investigated.

4) Both the reduction of yoke flap stiffness and pitch link stiffness increase whirl flutter speed. However, in general, their effects on aeroelastic stability are small.

5) The rotor rotational speed change has almost the same influence on aeroelastic stability as yoke chord stiffness (thus lag frequency).

6) As density decreases, damping values increase substantially due to lower dynamic pressure.

7) Decreasing the speed of sound, and thus increasing Mach number, reduces the wing beam mode damping slightly. In general, it has a small influence on aeroelastic stability over the velocity range analyzed.

8) In general, undersling increases whirl flutter speed, and precone reduces whirl flutter speed because of negative pitch–lag coupling.

9) Inclusion of unsteady aerodynamics in the analysis reduces whirl flutter speed.

10) Realistic airfoil tables instead of linear aerodynamics also reduces whirl flutter speed.

One of the most important findings was the need for extremely rigorous documentation and configuration control. The lesson is an old one and difficult to apply, particularly when trying to model the same physical system with different codes by different engineers. The payoff is implicit in the results: The predictions made by CAMRAD II and RCAS are nearly identical. The excellent match between the two codes came about neither easily nor automatically: Assiduous attention to detail was necessary throughout.

Note also that the results shown here were obtained for a purely hypothetical proprotor and wing/pylon, although an attempt was made to include all the key design parameters of realistic tiltrotor configurations. The next challenge is to apply them to an actual physical rotor with real experimental data. It is recommended that this research be extended to the WRATS model. The work reported in Refs. 19–22 was a major stimulus for the present paper, but showed the need for further improvement. It is hoped that the work reported here can serve as a foundation for improved analytical models of the WRATS and other proprotors.

Acknowledgments

The authors gratefully acknowledge Dr. Wayne Johnson of NASA Ames Research Center for his help and support with CAMRAD II and

Dr. Hossein Saberi of Advanced Rotorcraft Technology, Inc. (ART), for his help and support with RCAS.

References

[1]Hall, W. E., "Prop-Rotor Stability at High Advance Ratios," *Journal of the American Helicopter Society*, Vol. 11, (2), April 1966, pp. 11–26.

[2]Reed, W. H., III., "Review of Propeller-Rotor Whirl Flutter," NASA TR R-264, July 1967.

[3]Gaffey, T. M., "The Effect of Positive Pitch-Flap Coupling (Negative δ_3) on Rotor Blade Motion Stability and Flapping," *Journal of the American Helicopter Society*, Vol. 14, (2), April 1969, pp. 49–67.

[4]Johnson, W., "Dynamics of Tilting Proprotor Aircraft in Cruise Flight," NASA TN D-7677, May 1974.

[5]Johnson, W., "Analytical Modeling Requirements for Tilting Proprotor Aircraft Dynamics," NASA TN D-8013, July 1975.

[6]Kvaternik, R., "An Experimental and Analytical Investigation of Proprotor Whirl-Flutter," NASA TP 1047, December 1977.

[7]Srinivas, V., Chopra, I., and Nixon, M. W., "Aeroelastic Analysis of Advanced Geometry Tiltrotor Aircraft," *Journal of the American Helicopter Society*, Vol. 43, (3), July 1998, pp. 212–221.

[8]Barkai, S. M., Rand, O., Peyran, R. J., and Carlson, R. M., "Modeling and Analysis of Tilt-Rotor Aeromechanical Phenomena," *Mathematical and Computer Modelling*, Vol. 27, (12), June 1998, pp. 17–43.

[9]Parham, T., and Corso, L. M., "Aeroelastic and Aeroservoelastic Stability of the BA 609," 25th European Rotorcraft Forum, Rome, Italy, September 14–16, 1999.

[10]Acree, C. W., Jr., Peyran, R. J., and Johnson, W., "Rotor Design Options for Improving XV-15 Whirl-Flutter Stability Margins," NASA/TP-2004-212262, March 2004.

[11]Acree, C. W., Jr., "A CAMRAD II Model of the V-22 Rotor for Whirl-Flutter Analysis," NASA/TM-2004-212801, July 2004.

[12]Paik, J., Singh, R., Gandhi, F., and Hathaway, E., "Active Tiltrotor Whirl-Flutter Stability Augmentation Using Wing-Flaperon and Swash-Plate Actuation," *Journal of Aircraft*, Vol. 44, (5), September–October 2007.

[13]Piatak, D. J., Kvaternik, R. G., Nixon, M. W., Langston, C. W., Singleton, J. D., Bennett, R. L., and Brown, R. K., "A Parametric Investigation of Whirl-Flutter Stability on the WRATS Tiltrotor Model," *Journal of the American Helicopter Society*, Vol. 47, (2), April 2002, pp. 134–144.

[14]Zhang, J., and Smith, E. C., "Influence of Aeroelastically Tailored Wing Extensions and Winglets on Whirl Flutter Stability," 2nd Asian/Australian Rotorcraft Forum and 4th International Basic Research Conference on Rotorcraft Technology, Tianjin, People's Republic of China, September 8–11, 2013.

[15]Kim, T., Kim, J., Shin, S. J., and Kim, D. H., "Structural Design Optimization of a Tiltrotor Aircraft Composite Wing to Enhance Whirl Flutter Stability," *Composite Structures*, Vol. 95, January 2013, pp. 283–294.

[16]Newman, J., Parham, T., Johnson, C., and Popelka, D., "Wind Tunnel Test Results for a 0.2 Scale 4-Bladed Tiltrotor Aeroelastic Model," American Helicopter Society 70th Annual Forum Proceedings, Montréal, Canada, May 20–22, 2014.

[17]Masarati, P., Piatak, D. J., Quaranta, G., Singleton, J. D., and Shen, J., "Soft-Inplane Tiltrotor Aeromechanics Investigation Using Two Comprehensive Multibody Solvers," *Journal of the American Helicopter Society*, Vol. 53, (2), April 2008, pp. 179–192.

[18]Shen, J., Masarati, P., Roget, B., Piatak, D. J., Nixon, M. W., and Singleton, J. D., "Modeling a Stiff-Inplane Tiltrotor Using Two Multibody Analyses: A Validation Study," American Helicopter Society 64th Annual Forum Proceedings, Montreal, Canada, April 29–May 1, 2008.

[19]Shen, J., and Kang, H., "Comparison Study of Tiltrotor Whirl Flutter Using Two Rotorcraft Comprehensive Analyses," AHS Specialists' Conference on Aeromechanics Design for Vertical Lift, San Francisco, CA, January 20–22, 2016.

[20]Kang, H., Shen, J., and Kreshock, A. R., "Parametric Study of Tiltrotor Whirl Flutter Using Two Rotorcraft Comprehensive Analyses," American Helicopter Society 72nd Annual Forum Proceedings, West Palm Beach, FL, May 17–19, 2016.

[21]Kreshock, A. R., Thornburgh, R. P., Kang, H., and Yeo, H., "Validation of Comprehensive Modeling of the Wing Rotor Aeroelastic Test System," American Helicopter Society 72nd Annual Forum Proceedings, West Palm Beach, FL, May 17–19, 2016.

[22]Kreshock, A. R., and Yeo, H., "Tiltrotor Whirl-Flutter Stability Predictions Using Comprehensive Analysis," AIAA 2017-0639, AIAA Science and Technology Forum and Exposition, Grapevine, TX, January 9–13, 2017.

[23]Popelka, D., Sheffler, M., and Bilger, J., "Correlation of Test and Analysis for the 1/5-Scale V-22 Aeroelastic Model," *Journal of the American Helicopter Society*, Vol. 32, (2), April 1987, pp. 21–33.

[24]Settle, T. B., and Kidd, D. L., "Evolution and Test History of the V-22 0.2-Scale Aeroelastic Model," *Journal of the American Helicopter Society*, Vol. 37, (1), January 1992, pp. 31–45.

[25]Johnson, W., "Technology Drivers in the Development of CAMRAD II," American Helicopter Society Aeromechanics Specialist Meeting, San Francisco, CA, January 19–21, 1994.

[26]Saberi, H., Hasbun, M., Hong, J. Y., Yeo, H., and Ormiston, R. A., "Overview of RCAS Capabilities, Validations, and Rotorcraft Applications," American Helicopter Society 71st Annual Forum Proceedings, Virginia Beach, VA, May 5–7, 2015.

[27]Johnson, W., *Helicopter Theory*, Princeton University Press, Princeton, NJ, 1980.

[28]Petot, D., "Differential Equation Modeling of Dynamic Stall," *La Recherche Aerospatiale*, Number 1989-5 (corrections dated October 1990).

[29]Leishman, J. G., and Beddoes, T. S., "A Semi-Empirical Model for Dynamic Stall," *Journal of the American Helicopter Society*, Vol. 34, (3), July 1989, pp. 3–17.

[30]Johnson, W., "Rotorcraft Aerodynamics Models for a Comprehensive Analysis," American Helicopter Society 54th Annual Forum Proceedings, Washington, DC, May 20–22, 1998.

[31]Johnson, W., "Calculation of Tilt Rotor Aeroacoustic Model (TRAM DNW) Performance, Airloads, and Structural Loads," American Helicopter Society Aeromechanics Specialists Meeting, Atlanta, GA, November 13–15, 2000.

[32]Theodorsen, T., "General Theory of Aerodynamic Instability and the Mechanism of Flutter," NACA Report 496, 1935.

[33]Peters, D. A., Hsieh, M. A., and Torrero, A., "A State Space Airloads Theory for Flexible Airfoils," *Journal of the American Helicopter Society*, Vol. 52, (4), October 2007, pp. 329–342.

[34]Anonymous, "RCAS Theory Manual," USAAMCOM/AFDD TR 02-A-005, March 2005.

[35]Jain, R., Yeo, H., Bhagwat, M., and Ho, J. C., "An Assessment of RCAS Performance Prediction for Conventional and Advanced Rotor Configurations," *Journal of the American Helicopter Society*, **61**, 042005 (2016).

[36]Ho, J. C., and Yeo, H., "Assessment of Comprehensive Analysis Predictions of Helicopter Rotor Blade Loads in Forward Flight," *Journal of Fluids and Structures*, Vol. 68, January 2017, pp. 194–223.

[37]Yeo, H., Potsdam, M., and Ormiston, R. A., "Rotor Aeroelastic Stability Analysis Using Coupled Computational Fluid Dynamics/Computation Structural Dynamics," *Journal of the American Helicopter Society*, **56**, 042003 (2011).